This article has been accepted for publication in a future issue of this journal, but has not been fully edited. Content may change prior to final publication. Citation information: DOI 10.1109/TCSII.2021.3057388, IEEE Transactions on Circuits and Systems II: Express Briefs



# Real-Time Light Field Signal Processing using 4D/5D Linear Digital Filter FPGA Circuits

C. U. S. Edussooriya, C. Wijenayake, A. Madanayake, N. Liyanage, S. Premaratne, J. T. Vorhies, D. G. Dansereau, P. Agathoklis, and L. T. Bruton

***Abstract*—Light fields (LFs) and light field videos (LFVs) capture both angular and spatial variation of light rays emanating from scenes. This richness of information leads to novel applications such as post-capture refocusing, depth estimation and depth-velocity filtering which are not possible with images and videos. These capabilities come, however, with a significant increase in data to be processed. In order to fully exploit opportunities provided by LFs and LFVs, low-complexity signal processing algorithms that process LF and LFV data in real-time are required. In this paper, we survey such state-of-the-art algorithms, in particular for depth filtering, refocusing and denoising of LFs and depth-velcoty filtering for LFVs, and future directions for these real-time LF an LFV processing algorithms.**

***Index Terms*—Light fields, light field videos, multi-dimensional filters, real-time processing, FPGA.**

## I. Light Field Signal Processing and Applications

Recent advancements in light field (LF) sensing, processing, and display, some shown in Fig. 1, are opening exciting new possibilities for a next generation of applications. Commercial devices like the K-Lens adapter[1] are lowering the barrier to entry into the field, and the more than two decades of research since the first introduction of LFs [1], [2] are converging to enable unprecedented capabilities. These developments open new challenges and opportunities in LF signal processing. This article is a primer aiming to introduce the reader to the the state of the art and opportunities in this fascinating field.

The LF is a four-dimensional (4D) representation of light that describes variation in light intensity with ray position and direction [1], [3]. Unlike conventional two-dimensional (2D) imagery, the LF captures three-dimensional (3D) scene geometry and higher order effects including occlusions, specularity and refraction through transparent objects. The LF is the minimal representation that directly samples these behaviours.

**C. U. S. Edussooriya** is with the Dept. of Electronic and Telecommunication Eng., Univ. of Moratuwa, Sri Lanka (e-mail: chamira@uom.lk). **C. Wijenayake** is with the School of Information Technology and Electrical Eng., Univ. of Queensland, Australia (e-mail: c.wijenayake@uq.edu.au). **A. Madanayake** is with the Dept. of Electrical and Computer Eng., Florida International Univ., Florida, USA (email: amadanay@fiu.edu). **N. Liyanage** is with the School of Electrical Eng. and Telecommunications, Univ. of New South Wales, Australia (e-mail: n.kanankeliyanage@unsw.edu.au). **J. T. Vorhies** is with the the Dept. of Electrical and Computer Eng., The Univ. of Akron, Ohio, USA (e-mail: jrv19@zips.uakron.edu). **D. G. Dansereau** is with the Sydney Institute for Robotics and Intelligent Systems, Univ. of Sydney, Australia (e-mail: donald.dansereau@sydney.edu.au). **S. Premaratne** and **P. Agathoklis** are with the Dept. of Electrical and Computer Eng., Univ. of Victoria, Canada (e-mail:sandunipremaratne@uvic.ca, pan@ece.uvic.ca). **L.T. Bruton** is with the Dept. of Electrical and Computer Eng., Univ. of Calgary, Canada (e-mail: bruton@ucalgary.ca).

[1]https://www.k-lens.de/

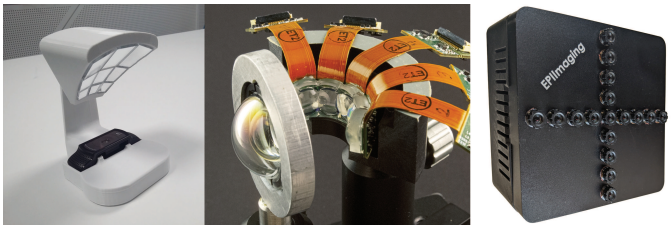


Fig. 1. Emerging LF devices with new capabilities: (left) easily fabricated adapters [12] are increasing access to hardware, (center) spherical lenses allow single-aperture wide-field-of-view [13] and (right) devices like the EPIModule from EPIImaging LLC tightly integrate sensing, compute, and FPGA fabric.

LF capture has been shown to offer advantages in seeing through scattering media, ignoring occluders, and gathering more light in low-light scenarios [4]–[7]. The LF structure also enables closed-form, low-latency approaches to problems conventionally requiring complex, iterative solutions. Examples include depth estimation, visual odometry, and change detection [8]–[11]. This capability is especially relevant in enabling low-latency solutions that take advantage of parallel processing architectures.

Recent work has pushed towards real-time, embedded applications of LF capture, processing, and display. Developments like Google's light field video (LFV) capture [14] and the highly integrated capture-and-compute EPIModule device depicted in Fig. 1 are paving the way for practical deployment in challenging scenarios. For example, emerging 6G wireless networks, multi-agent robotics, and unmanned aerial systems may utilize computer vision systems based on LF preprocessing before machine learning algorithms, such as object recognition based on deep convolutional neural network (CNN) (e.g., YOLOv4 [15]) are applied.

The utilization of embedded 4D filters for depth-based image enhancement, occlusion removal, and five-dimensional (5D) filters for depth-velocity filtering reduces overall complexity of processing pipelines. By combining 6G wireless concepts such as holographic massive multi-input-multi-output (MIMO) with 4D/5D embedded LF signal processing, we can achieve scene sensing with low-latency occlusion removal. Computer vision enables wireless access points to locate users in a crowd based on LF processing for occlusion removal in concert with CNN-based facial recognition [16], [17].

LF display is also developing rapidly, and there are now commercially available autostereoscopic displays like the ones from Light Field Lab and FoVI3D[2]. Worn virtual/mixed/augmented reality (XR) displays have been in de-

[2]https://www.lightfieldlab.com/ and http://www.fovi3d.com/

This article has been accepted for publication in a future issue of this journal, but has not been fully edited. Content may change prior to final publication. Citation information: DOI 10.1109/TCSII.2021.3057388, IEEE Transactions on Circuits and Systems II: Express Briefs



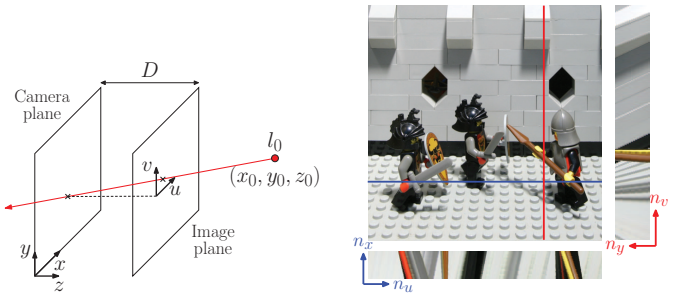


(a) (b)

Fig. 2. The two-plane parameterization of a Lambertian point source; (b) A SAI of the "Kinghts" LF of the Stanford dataset [21], and EPI representations, where different depths map to lines with different gradients.

velopment for over half a decade [18], with worn 4D displays generally seen as the ultimate goal for immersive experiences.

These developments point the way forward for applications spanning live and cinematic mixed reality, and autonomous perception including robotic imaging for driving, drone delivery, and manipulation. There are however unmet challenges in handling the vast quantities of data associated with 4D LF capture, and there is a pressing need for algorithms and architectures that can unlock the potential for low-power, low-latency embedded LF processing. In the case of imaging systems, typical LF processing pipelines include LF acquisition and rendering followed by denoising and various depth/velocity based filtering techniques as pre-processing, feeding in to compression and/or machine learning back-ends for numerous classification and detection tasks. This paper focuses on state-of-the-art in LF front-end processing which are mostly linear algorithms suitable for low-complexity real-time implementations and highlights some of the opportunities and challenges associated with the next generation of applications.

## II. Signal Model and Spectral Properties of LFs

The design of linear and shift-invariant filters for 4D LF and 5D LFV processing is based on the shape and orientation of region of support (ROS) of the spectra of LFs and LFVs. We employ the most widely used two-plane parameterization[3] [1], where a light ray is parameterized by its intersections with two planes: the camera plane and the image plane, which sample *angular information* and *spatial information* of light rays emanating from a scene, respectively.

### A. Spectrum of a Light Field Containing Lambertian Objects

We first consider an LF containing a Lambertian point source[4] having an intensity $l_0$ (see Fig. 2(a)). Such a Lambertian point source is represented as a plane of constant value $l_0$ in a discrete-domain LF $l_p(\mathbf{n}_4)$ (see Fig. 2(b)), where $\mathbf{n}_4 = (n_x, n_y, n_u, n_v) \in \mathbb{Z}^4$, i.e., [22]

$$l_p(\mathbf{n}_4) = l_0\, \delta(mn_x\Delta_x + n_u\Delta_u - mx_0) \times \delta(mn_y\Delta_y + n_v\Delta_v - my_0), \quad (1)$$

where $m = \frac{D}{z_0}$, $\Delta_i$, $i = x, y, u, v$, is the sampling interval along the dimension $i$, $(x_0, y_0, z_0) \in \mathbb{R}^2 \times \mathbb{R}^+$ is the position of the source, $D$ is the distance between the camera and image planes and $\delta(\cdot)$ is the one-dimensional discrete-domain impulse function. In this case, the ROS $\mathcal{R}_p$ of the spectrum $L_p(\boldsymbol{\omega}_4)$, where $\boldsymbol{\omega}_4 = (\omega_x, \omega_y, \omega_u, \omega_v) \in \mathbb{R}^4$, inside the principal Nyquist hypercube $\mathcal{N}_4$ ($\triangleq \{\boldsymbol{\omega}_4 \in \mathbb{R}^4 \mid -\pi \leq \omega_i < \pi, i = x, y, u, v\}$) is given by $\mathcal{R}_p = \mathcal{H}_{xu} \cap \mathcal{H}_{yv}$ [22], [23], where

$$\mathcal{H}_{xu} = \left\{ \boldsymbol{\omega} \in \mathbb{R}^4 \middle| \omega_x - \left(\frac{m\Delta_x}{\Delta_u}\right)\omega_u = 0 \right\} \quad (2a)$$

$$\mathcal{H}_{yv} = \left\{ \boldsymbol{\omega} \in \mathbb{R}^4 \middle| \omega_y - \left(\frac{m\Delta_y}{\Delta_v}\right)\omega_v = 0 \right\}. \quad (2b)$$

Here, the ROS $\mathcal{R}_p$ is a plane through the origin of $\boldsymbol{\omega}_4$ inside $\mathcal{N}_4$. Importantly, the orientation of $\mathcal{R}_p$ depends *only on the depth* $z_0$ of the Lambertian point source. Even with the constraints such as the finite sizes of the camera and image planes and non Lambertian reflections, which are not considered in this analysis for simplicity, the spectral ROS predominantly occupies the region defined by the ROS $\mathcal{R}_p$ [24], [25].

In the case of a Lambertian object occupying a *volumetric region* with a depth range $z_0 \in [d_{min}, d_{max}]$, the spectral ROS becomes $\mathcal{R}_o$ as $\mathcal{R}_o = \bigcup_{z_0} \mathcal{R}_p = \bigcup_{z_0} (\mathcal{H}_{xu} \cap \mathcal{H}_{yv})$ [23], [26], [37], which corresponds to a *hyperfan* inside $\mathcal{N}_4$ [5].

### B. Spectrum of a Light Field Video Containing Lambertian Objects Moving with Constant Velocity and Constant Depth

We now consider modeling of a Lambertian point source moving with a constant velocity $\mathbf{V} = [V_x, V_y, V_z]^{\mathrm{T}}$ in an LFV. This may be considered as a sequence of LFs, in which the point source is located at different depths. Because of this depth variation, the point source is represented as a hypersurface of constant value $l_0$ in an LFV [27], [28]. When $V_z = 0$, i.e., the point source moves at a constant depth $z_0$, the discrete-domain LFV $lv_p(\mathbf{n}_5)$, where $\mathbf{n}_5 = (n_x, n_y, n_u, n_v, n_t) \in \mathbb{Z}^5$, can be expressed as [27], [28]

$$lv_p(\mathbf{n}_5) = l_0\, \delta(mn_x\Delta_x + n_u\Delta_u + a_x n_t\Delta_t - mx_0) \times \delta(mn_y\Delta_y + n_v\Delta_v + a_y n_t\Delta_t - my_0), \quad (3)$$

where $m = \frac{D}{z_0}$, $a_x = \frac{-DV_x}{z_0}$ and $a_y = \frac{-DV_y}{z_0}$, $(x_0, y_0, z_0) \in \mathbb{R}^2 \times \mathbb{R}^+$ is the position of the Lambertian point source at time $n_t = 0$, and $\mathbf{A} = [a_x, a_y, 0]^{\mathrm{T}}$ denotes the apparent velocity. Note that the point source is represented as hyperplane of constant value $l_0$ in the LFV $lv_p(\mathbf{n}_5)$. In this case, the ROS $\mathcal{P}_p$ of the spectrum $LV_p(\boldsymbol{\omega}_5)$, where $\boldsymbol{\omega}_5 = (\omega_x, \omega_y, \omega_u, \omega_v, \omega_t) \in \mathbb{R}^5$, inside the principal Nyquist hypercube $\mathcal{N}_5$ ($\triangleq \{\boldsymbol{\omega}_5 \in \mathbb{R}^5 \mid -\pi \leq \omega_i < \pi, i = x, y, u, v, t\}$) is given by $\mathcal{P}_p = \mathcal{H}_{xu} \cap \mathcal{H}_{yv} \cap \mathcal{H}_{uvt}$ [27], [28], where $\mathcal{H}_{xu}$ and $\mathcal{H}_{yv}$ are given in (2a) and (2b), and

$$\mathcal{H}_{uvt} = \left\{ \boldsymbol{\omega}_5 \in \mathbb{R}^5 \middle| \omega_t - \left(\frac{a_x\Delta_t}{\Delta_u}\right)\omega_u - \left(\frac{a_y\Delta_t}{\Delta_v}\right)\omega_v = 0 \right\}.$$

The ROS $\mathcal{P}_p$ is a plane through the origin of $\boldsymbol{\omega}_5$ inside $\mathcal{N}_5$ of which the orientation of depends *only on the depth* $z_0$ *and the apparent velocity* $\mathbf{A}$ of the Lambertian point source [28].

[3]Two other possible LF parameterizations are the two-sphere parameterization [19], [20] and the sphere-plane parameterization [19]

[4]A Lambertian point source is an isotropic light source.

This article has been accepted for publication in a future issue of this journal, but has not been fully edited. Content may change prior to final publication. Citation information: DOI 10.1109/TCSII.2021.3057388, IEEE Transactions on Circuits and Systems II: Express Briefs



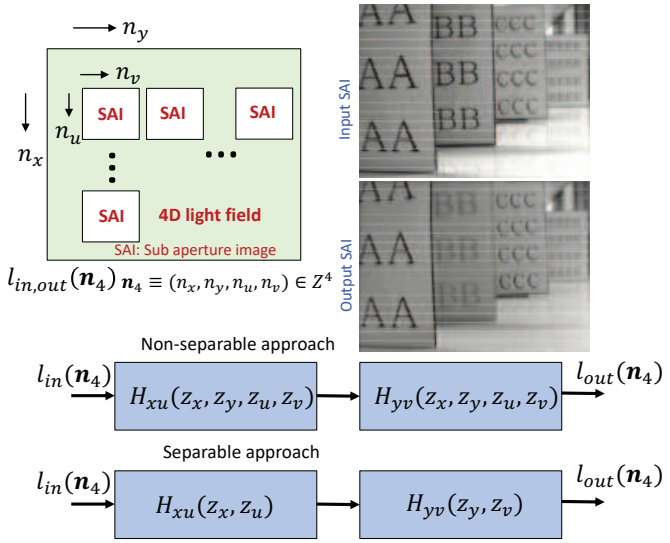


Fig. 3. LF depth filtering with 4D spatial domain processing.

In the case of a Lambertian object moving with a constant velocity $\mathbf{V} = [V_x, V_y, 0]^{\mathrm{T}}$ and occupying a volumetric region with a depth range $z_0 \in [d_{min}, d_{max}]$, we can deduce the spectral ROS $\mathcal{P}_o$ as $\mathcal{P}_o = \bigcup_{z_0} \mathcal{P}_p = \bigcup_{z_0} (\mathcal{H}_{xu} \cap \mathcal{H}_{yv} \cap \mathcal{H}_{uvt})$ which corresponds to a *hyperfan* inside $\mathcal{N}_5$ [27], [28].

## III. Depth Enhancing and Refocusing Filters

Following the properties of spectral ROS LFs outlined above, 4D linear and shift-invariant filters can be designed for selective filtering of one or many regions of a scene based on depth [22], [29], [30]. Such depth filtering is typically achieved by employing 4D linear and shift-invariant filters having hyperplanar or hyperfan passbands with appropriate orientation in $\mathcal{N}_4$. Post-capture refocusing can be seen as a special case of depth filtering where the stopband objects are blurred than being heavily attenuated.

Fig. 3 shows two commonly used architectures for 4D depth filtering. While the non-separable approach employs 4D filters, based on the partially separable nature of the spectral ROS of a Lambertian object, the separable approach employs a cascade of 2D filters, each operating on the entire 4D data hypercube. The 4D input $l_{in}(\mathbf{n}_4)$ is typically organised as an array of 2D SAIs, which is processed by the depth filter to produce $l_{out}(\mathbf{n}_4)$. Depending on the application and subsequent stages of processing, either the entire 4D output or a set of selected SAIs of the output can be computed. Fig. 3 also shows an example SAI of the input and output in the case of a multi-depth focusing scenario, where the letter surfaces A and C are in focus. A variety of multidimensional filter design techniques can be employed to design $H_{xu}(z_x, z_u)$ and $H_{yv}(z_y, z_v)$ and different design choices (such as finite-extent impulse response (FIR) and infinite-extent impulse response (IIR)) are based on the application and computational resources. Table I provides a summary of some previously reported 4D depth filters.

### A. Four-Dimensional FIR Filters

The depth filtering concept was first demonstrated in [29] using an FIR filter having hyperplanar passband, where a planar region at a constant depth of a scene has been enhanced. In [4], [5], an FIR filter having a hyperfan passband was proposed, which can be employed to enhance a volumetric region of a scene. This filter provides excellent performance in LF refocusing and denoising. FIR hyperfan filters having sparse coefficients are proposed in [35]–[37], which provide significant reduction in computational complexity with almost negligible degradation in output quality and provide similar performance in refocusing and depth filtering compared to [4], [5]. In particular, the FIR filter designs proposed in [36] and [37] are optimal in the minimax and least-squares senses, respectively. In [31] and [32], low-complexity FIR filters were implemented on Xilinx Spartan-6 FPGAs for real-time planar refocusing of LFs. Furthermore, the sparse FIR filter designs [36] and [37] have a good potential to be implemented on FPGAs for real-time volumetric refocusing of LFs.

TABLE I
Summary of the Architectures of 4D Depth Filters.

| Architecture | Separable | Type/Passband |
|---|---|---|
| [29] | × | FIR/hyperplanar |
| [22] | × | IIR/hyperplanar |
| [31], [32] | ✓ | FIR/hyperplanar |
| [33], [34] | ✓ | IIR/multiple hyperplanar |
| [4], [5] | ✓ | FIR/hyperfan |
| [26] | ✓ | IIR/hyperfan |
| [35], [36] | ✓ | sparse FIR/hyperfan |
| [37] | ✓ | sparse FIR/multiple hyperfan |

### B. Four-Dimensional IIR Filters

In order to achieve extremely low computational complexity[5], 4D IIR filters have been employed in LF depth filtering [22], [26], [33], [34]. The fundamental idea to employ separable multi-dimensional IIR filters to realize higher dimensional hyperplanar passbands is described in [38], [39] for the 3D case and was extended to 4D in [22], [30]. The coefficients of these filters are obtained by following filter synthesis based on the concept of multidimensional passive network resonance [38], [39], which leads to practical-bounded-input-bounded-output stable [40] 4D IIR filters. Typical design process begins with selecting an appropriate 2D/4D passive prototype network (containing inductors and capacitors with at least one resisitive termination) having prescribed transfer function and passband characteristics in the 4D Laplace domain, and applying 4D (normalized) bilinear transform to obtain the corresponding 4D $\mathbf{z}$-domain transfer function, which after simplifications, yields the required coefficients and 4D input-output difference equations. Such 4D filters can be designed to have one or many hyperplanar or hyperfan passbands[6] in $\mathcal{N}_4$, hence can be used to perform depth filtering over one or many desired depths. Typically, with such 4D IIR approaches, zero-phase filtering is employed to alleviate the effects of non-linear phase response of these filters. Detailed information on such low-complexity 4D IIR filters can be found in [22], [26], [33], [34], [41].

[5] A 4D FIR filter or order $20\times20\times20\times20$ would required $21^4$ multipliers whereas an equally selective 4D IIR filter of order $1\times1\times1\times1$ would require 15 multipliers per output sample

[6] Here, a hyperplanar passband shape leads to depth filtering and hyperfan passband leads to volumetric filtering.

This article has been accepted for publication in a future issue of this journal, but has not been fully edited. Content may change prior to final publication. Citation information: DOI 10.1109/TCSII.2021.3057388, IEEE Transactions on Circuits and Systems II: Express Briefs



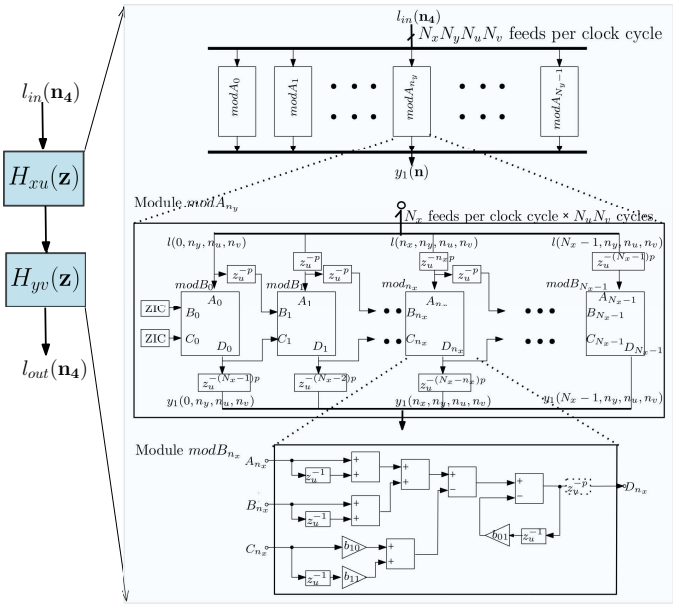


Fig. 4. Semi-systolic hardware architecture SFG$[N_x, N_y, 1, 1]$ of $H_{xu}(z_x, z_u)$ in 4D IIR depth filter with single passband [34].

### C. Hardware Architectures

The above 4D depth filters can be mapped into digital hardware architectures to exploit massive hardware parallelism offered by FPGAs. The underlying 4D input-output difference equations can be mapped into suitable signal flow graphs (SFGs) to obtain hardware architectures denoted by SFG$[J_{n_x}, J_{n_y}, J_{n_u}, J_{n_v}]$, where $1 \leq J_i \leq N_i$ denotes the level of parallelism in each dimension $n_i$, $i \in \{x, y, u, v\}$, where $(N_x \times N_y \times N_u \times N_v)$ denotes the LF size. Here, $J_i = 1$ and $J_i = N_i$ imply sequential and fully-parallel (i.e., systolic) processing of samples along the dimension $n_i$, respectively. For example, SFG$[1, 1, 1, 1]$ implies a fully-sequential architecture with a centralized processing module taking a one-dimensional input obtained by raster scanning the 4D LF, while SFG$[N_x, N_y, 1, 1]$ implies a semi-systolic architecture with dedicated processing element for each location $(n_x, n_y)$ on the camera plane which sequentially processes input samples along $n_u$ and $n_v$ dimensions. The level of parallelism is a design choice to be made based on the required real-time throughput and available hardware resources. Design techniques such as fine-grain/look-ahead pipelining and J-unfolding [42] can be employed to optimize the implementations in terms of critical path delay and throughput at the cost of hardware. Implementation of IIR hyperplanar depth filter [22] was done following a fully sequential architecture SFG$[1, 1, 1, 1]$ in [43]–[47] and a semi-systolic architecture SFG$[4, 4, 1, 1]$ in [48]. Fig. 4 shows semi-systolic hardware architecture of 4D IIR multi-passband depth filter in [34] for single passband case. Performance of such hardware designs is typically benchmarked using metrics such as the critical path delay ($T_{\text{CPD}}$), maximum frequency of operation $F_{\text{MAX}} < 1/T_{\text{CPD}}$, real-time throughput $F_{\text{SAMP}} = KF_{\text{MAX}}$ (where $K$ depends on the degree of parallel processing) and FPGA resource consumption. Design challenges include optimizing the level of pipelining and parallel processing for the best real-time throughout while reducing the overall hardware complexity.

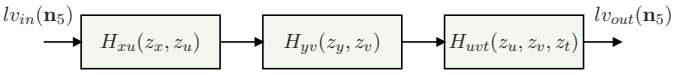


Fig. 5. The architecture of a 5D depth-velocity filter.

## IV. Depth-Velocity Filtering

It is evident from the spectral ROS presented in II-B that the objects moving with different constant velocities and different depths ideally have non-overlapping spectral ROSs, except at the origin, inside $\mathcal{N}_5$. Therefore, by employing a 5D filter of which passband encompasses the spectral ROSs of desired moving objects of interest (OOIs) and the stopband encompasses the spectral ROSs of moving or static interfering objects, OOIs can be enhanced while attenuating interfering objects. Such 5D *depth-velocity* filters [27], [28], can be considered as a combination of 4D depth filters (see Sec. III) and 3D velocity filter applied to videos [38], [49]–[53].

Exploiting the partial-separability of the spectral ROS $\mathcal{P}_p$ of a Lambertian point source, depth-velocity filters are designed as a cascade of three filters as shown in Fig. 5. In this case, the transfer function of the depth-velocity filter $H(\mathbf{z})$, $\mathbf{z} = [z_x, z_y, z_u, z_v, z_t]^{\mathrm{T}} \in \mathbb{C}^5$, can be expressed as

$$H(\mathbf{z}) = H_{xu}(z_x, z_u)H_{yv}(z_y, z_v)H_{uvt}(z_u, z_v, z_t). \quad (4)$$

Here, $H_{xu}(z_x, z_u)$ and $H_{yv}(z_y, z_v)$ realize a depth filter with passbands encompassing the hypervolumes $\bigcup_{z_0} \mathcal{H}_{xu}$ and $\bigcup_{z_0} \mathcal{H}_{yv}$, respectively, and $H_{uvt}(z_u, z_v, z_t)$ realizes a velocity filter with passband encompassing the hypervolume $\bigcup_{z_0} \mathcal{H}_{uvt}$.

### A. 5D Depth-Velocity Filter Designs

The filters $H_{xu}(z_x, z_u)$, $H_{yv}(z_y, z_v)$ and $H_{uvt}(z_u, z_v, z_t)$ can be designed as FIR or IIR filters with hyperplanar or hyperfan passbands, see Table II for a summary. Here, the FIR depth-velocity filters proposed in [28] and [54] provide very good performance in enhancing OOIs compared to the IIR depth-velocity filters proposed in [55]. However, the IIR depth-velocity filter [55], designed with first-order filters [38], [39], has an extremely low computational complexity. Compared to the FIR depth-velocity filter having hyperplanar passbands [28], that having hyperfan passbands [54] provides better performance in enhancing OOIs with the same computational complexity because the latter provides a better selectivity at frequencies near the origin in $\mathcal{N}_5$. The depth-velocity filter in [56] employed a combination of hyperplanar IIR and a hyperfan FIR filters. This filter provides better enhancement of OOIs compared to filters [28] and [55] and has a computational complexity lower compared to [28], however, higher compared to [55]. Recently, the depth-velocity filter in [56] has been extended to enhance multiple OOIs moving with different constant velocities and depths in [57].

### B. Hardware Architectures for 5D Depth-Velocity Filters

An FPGA architecture for the IIR depth-velocity filter in [55] has been presented in [58]. This implementation employs a semi-systolic array architecture with direct-form I realizations for $H_{xu}(z_x, z_u)$, $H_{yv}(z_y, z_v)$ and $H_{uvt}(z_u, z_v, z_t)$.

TABLE II
SUMMARY OF THE ARCHITECTURES OF 5D DEPTH-VELOCITY FILTERS.

| Architecture | $H_{xu}(z_x, z_u)$ and $H_{yv}(z_y, z_v)$ | $H_{uvt}(z_u, z_v, z_t)$ |
|---|---|---|
| [28] | FIR hyperplanar | FIR hyperplanar |
| [55] | IIR hyperplanar | IIR hyperplanar |
| [56] | IIR hyperplanar | FIR hyperfan |
| [54] | FIR hyperfan | FIR hyperfan |

Thanks to the extremely low computational complexity of the first-order IIR hyperplanar filters, this implementation on a Xilinx Virtex-7 FPGA implies a throughput of $467$ LFV frames/s for an input LFV frames of size $9 \times 9 \times 220 \times 360$. Because of the better performance of FIR depth-velocity filters compared to IIR counterparts, future work needs to consider FPGA implementations of such FIR filters. Depth-velocity FIR filters with sparse coefficients, such as extensions of those proposed for LF processing [36], [37], have a great potential to be implemented in FPGAs for real-time processing.

## V. Light Field Denoising Algorithms and Architectures for Real-Time Processing

Denoising of LFs is a fundamental preprocessing step required for computer vision algorithms. LF denoising algorithms can be mainly categorized into three classes: image and video denoising methods extended for LFs; linear methods; and non-linear methods unique to LFs. The first approach is to denoise each SAI individually using an off-the-shelf 2D image denoising algorithm. A summary of algorithms that can be used for this straightforward but time-consuming approach can be found in [59] and [60]. However, these methods do not utilize the angular correlations between different SAIs. On the other hand, state-of-the-art video denoising algorithms such as V-BM3D [61] and V-BM4D [62] can be utilized by reshaping the LF into a sequence of SAIs or EPIs [63] [64], however, they are far from being real-time and are not suitable for LFVs.

The nonlinear denoising methods specifically developed for LFs include majority of the recently proposed LF denoising techniques. LFBM5D method proposed in [65] extends the V-BM3D denoising algorithm [61] to LFs, such that angular redundancies are utilized. An LF denoising method using two CNNs is proposed in [66]. In [67], a tensor-based LF denoising method was proposed, which utilizes super-resolution to eliminate sub-pixel misalignment between different SAIs. In [68] a LF denoising method using anisotropic diffusion based on partial differential equations was proposed. Recently, a denoising method was proposed in [69] by extending the intrinsic tensor sparsity model utilized for multispectral image denoising. Despite excellent denoising performance, these nonlinear methods do not process LFs in real time.

The class of linear denoising methods has the best potential to be implemented in real-time. These methods exploit the spectral sparsity of LFs, i.e., the hyperfan ROS of corresponding to objects in an LF takes a small fraction in $\mathcal{N}_4$. These techniques employ 4D hyperplanar [22] or 4D hyperfan [4], [70], [71] filters. In particular, the denoising method proposed in [71] provides very good denoising performance with real-time processing. This method employs a mixed-domain implementation, i.e., $(\omega_x, \omega_y)$ frequency domain and $(n_u, n_v)$ spatial domain, and further exploits spectral sparsity with selective filtering approach [70], [71]. The semi-systolic hardware architecture of this algorithm implemented on a Xilinx Vertex-7 FPGA implies a throughput of $25$ LF/s for an LF of size $11 \times 11 \times 625 \times 434$.

## VI. Adaptive 4D Depth/5D Depth-Velocity Filters

For LF applications in the fields of robotics and autonomous vehicles, scene structure is constantly changing. In computer vision tasks where an OOI needs to be tracked across a dynamic scene, 2D imaging systems show decreased performance due to occlusions [72]. In this situation, 4D depth and 5D depth-velocity filters can be used as a pre-processing step for image segmentation, object detection, facial recognition, event detection and avoidance, or visual surveillance. When the OOI also varies in relative depth and velocity to the camera system, constant depth and depth-velocity filters discussed in Secs. III and IV, respectively, are not sufficient to extract an OOI, and adaptive versions of these filters are required.

In [73], an adaptive 4D IIR depth filtering algorithm is devised for enhancement of OOIs. This algorithm incorporates feedback from previous LFV frames to refine the ROS for an OOI as its relative depth changes over time. This refinement is performed by extracting an EPI from an LF, and searching its spectra for a reasonable candidate of $\mathcal{R}_o$. The filter is re-tuned to $\mathcal{R}_o$, shifting the plane of focus onto the OOI. A massively-parallel filter bank architecture is used to perform the search, allowing for an efficient implementation on an FPGA [74].

A 5D IIR adaptive filter was proposed in [75] to enhance objects moving at non-constant depths and with non-constant velocities. This filter has been designed using the first-order IIR filters as in [52], and the coefficients are adapted at each frame based on the instant depth and velocity. Due to the low computational complexity, this filter is a promising candidate for real-time LFV processing on FPGAs.

Computer vision tasks in real-time systems require low-latency solutions to enable adaptation in complex environments. While state-of-the-art learning-based algorithms often provide exceptional results [76]–[78], they are not realizable in resource-constrained systems such as field robotics. Adaptive depth/depth-velocity filters provide a low cost, low-latency solution to lessen the computational power required by more complex computer vision algorithms.

## VII. Conclusions

This paper presented a tutorial overview of recently proposed 4D/5D linear filtering techniques suitable for real-time processing of computationally intensive LFs, with specific emphasis on depth and velocity based filtering and denoising. Blending of powerful imaging and sensing capabilities of LFs and LFVs with emerging embedded, edge and internet of things applications has huge potential to benefit numerous areas including robotic vision and autonomous navigation. Low-complexity linear filtering algorithms and hardware architectures enable real-time preprocessing front-ends in LF imaging pipelines and provide potential integration with more computationally intensive secondary (non-linear) processing such as deep learning back-ends.

## REFERENCES


[1] M. Levoy and P. Hanrahan, "Light field rendering," in *Proc. Annu. Conf. Comput. Graph. (SIGGRAPH)*, 1996, pp. 31–42.

[2] E. Adelson and J. Bergen, "The plenoptic function and the elements of early vision," *Computational Models of Visual Processing*, pp. 3–20, 1991.

[3] I. Ihrke, J. Restrepo, and L. Mignard-Debise, "Principles of light field imaging," *IEEE Signal Process. Mag.*, vol. 1053, no. 5888/16, 2016.

[4] D. G. Dansereau, D. L. Bongiorno, O. Pizarro, and S. B. Williams, "Light field image denoising using a linear 4D frequency-hyperfan all-in-focus filter," *Proc. SPIE*, vol. 8657, p. 86570P, 2013. [Online]. Available: http://proceedings.spiedigitallibrary.org/proceeding.aspx?doi=10.1117/12.2002239

[5] D. G. Dansereau, O. Pizarro, and S. B. Williams, "Linear volumetric focus for light field cameras," *ACM Trans. Graph.*, vol. 34, no. 2, pp. 15:1–15:20, Feb. 2015.

[6] A. Bajpayee, A. H. Techet, and H. Singh, "Real-time light field processing for autonomous robotics," in *2018 IEEE/RSJ Int. Conf. Intell. Robots and Syst. (IROS)*. IEEE, 2018, pp. 4218–4225.

[7] Y. Ni, J. Chen, and L. Chau, "Reflection removal based on single light field capture," in *2017 IEEE Int. Symp. on Circuits Systems*, May 2017, pp. 1–4.

[8] E. H. Adelson and J. Y. A. Wang, "Single Lens Stereo with a Plenoptic Camera," *IEEE Transactions on Pattern Analysis and Machine Intelligence (TPAMI)*, vol. 14, no. 2, 1992.

[9] F. Dong, S.-H. Ieng, X. Savatier, R. Etienne-Cummings, and R. Benosman, "Plenoptic cameras in real-time robotics," *Int. J. Robot. Res.*, vol. 32, no. 2, pp. 206–217, Feb. 2013.

[10] D. G. Dansereau, S. B. Williams, and P. I. Corke, "Closed-form change detection from moving light field cameras," in *IROS Workshop on Alternative Sensing for Robotic Perception*. IEEE, Sep. 2015.

[11] J. Chen, J. Hou, Y. Ni, and L. Chau, "Accurate light field depth estimation with superpixel regularization over partially occluded regions," *IEEE Trans. on Image Proc.*, vol. 27, no. 10, pp. 4889–4900, Oct 2018.

[12] D. Tsai, D. G. Dansereau, S. Martin, and P. Corke, "Mirrored light field video camera adapter," Queensland University of Technology, Tech. Rep., Dec. 2016.

[13] G. M. Schuster, D. G. Dansereau, G. Wetzstein, and J. E. Ford, "Panoramic single-aperture multi-sensor light field camera," *Optics Express*, vol. 27, no. 26, pp. 37 257–37 273, 2019.

[14] M. Broxton, J. Flynn, R. Overbeck, D. Erickson, P. Hedman, M. Duvall, J. Dourgarian, J. Busch, M. Whalen, and P. Debevec, "Immersive light field video with a layered mesh representation," *ACM Transactions on Graphics (TOG)*, vol. 39, no. 4, pp. 86–1, 2020.

[15] A. Bochkovskiy, C.-Y. Wang, and H.-Y. M. Liao, "YOLOv4: Optimal speed and accuracy of object detection," *arXiv preprint arXiv:2004.10934*, 2020.

[16] M. Alrabeiah, A. Hredzak, and A. Alkhateeb, "Millimeter wave base stations with cameras: Vision-aided beam and blockage prediction," in *2020 IEEE 91st Vehicular Technology Conference (VTC2020-Spring)*, May 2020, pp. 1–5.

[17] M. Alrabeiah, A. Hredzak, Z. Liu, and A. Alkhateeb, "Viwi: A deep learning dataset framework for vision-aided wireless communications," in *2020 IEEE 91st Vehicular Technology Conference (VTC2020-Spring)*, 2020, pp. 1–5.

[18] F.-C. Huang, K. Chen, and G. Wetzstein, "The light field stereoscope: immersive computer graphics via factored near-eye light field displays with focus cues," *ACM Transactions on Graphics (TOG)*, vol. 34, no. 4, p. 60, 2015.

[19] E. Camahort, A. Lerios, and D. Fussell, "Uniformly sampled light fields," Univ. Texas at Austin, Austin, TX, Tech. Rep. TR98-09, 1998.

[20] I. Ihm, S. Park, and R. K. Lee, "Rendering of spherical light fields," in *Proc. Pacific Conf. Comput. Graph. Appl.*, 1997, pp. 59–68.

[21] Computer Graphics Laboratory, Stanford University. (2008) The (New) Stanford Light Field Archive. [Online]. Available: http://lightfield.stanford.edu/lfs.html

[22] D. Dansereau and L. Bruton, "A 4D frequency-planar IIR filter and its application to light field processing," in *Proc. IEEE Int. Symp. Circuits Syst.(ISCAS)*, vol. 4, 2003, pp. 476–479.

[23] J.-X. Chai, X. Tong, S.-C. Chan, and H.-Y. Shum, "Plenoptic sampling," in *Proc. Annu. Conf. Comput. Graph. (SIGGRAPH)*, 2000, pp. 307–318.

[24] M. N. Do, D. Marchand-Maillet, and M. Vetterli, "On the bandwidth of the plenoptic function," *IEEE Trans. Image Process.*, vol. 21, no. 2, pp. 708–717, Feb. 2012.

[25] C. Gilliam, P.-L. Dragotti, and M. Brookes, "On the spectrum of the plenoptic function," *IEEE Trans. Image Process.*, vol. 23, no. 2, pp. 502–516, Feb. 2014.

[26] D. Dansereau and L. T. Bruton, "A 4-D dual-fan filter bank for depth filtering in light fields," *IEEE Trans. Signal Process.*, vol. 55, no. 2, pp. 542–549, Feb. 2007.

[27] C. U. S. Edussooriya, "Low-complexity multi-dimensional filters for plenoptic signal processing," Ph.D. dissertation, Department of Electrical and Computer Engineering, University of Victoria, Victoria, BC, Canada, 2015.

[28] C. U. S. Edussooriya, D. G. Dansereau, L. T. Bruton, and P. Agathoklis, "Five-Dimensional Depth-Velocity Filtering for Enhancing Moving Objects in Light Field Videos," *IEEE Transactions on Signal Processing*, vol. 63, no. 8, pp. 2151–2163, 2015.

[29] A. Isaksen, L. McMillan, and S. J. Gortler, "Dynamically reparameterized light fields," in *Proc. Annu. Conf. Comput. Graph. (SIGGRAPH)*, 2000, pp. 297–306.

[30] D. G. Dansereau, "4D light field processing and its application to computer vision," Master's thesis, Department of Electrical and Computer Engineering, University of Calgary, Calgary, AB, Canada, 2003.

[31] C. Hahne and A. Aggoun, "Embedded FIR filter design for real-time refocusing using a standard plenoptic video camera," in *Proc. SPIE Electron. Imag.*, vol. 9023, 2014, pp. 902 305–1–902 305–12.

[32] C. Hahne, A. Lumsdaine, A. Aggoun, and V. Velisavljevic, "Real-time refocusing using an FPGA-based standard plenoptic camera," *IEEE Trans. Ind. Electron.*, vol. 65, no. 12, pp. 9757–9766, Dec. 2018.

[33] N. Liyanage, C. Wijenayake, C. Edussooriya, A. Madanayake, P. Agathoklis, E. Ambikairajah, and L. Bruton, "Low-complexity 4-D IIRfilters for Multi-depth filtering and Occlusion suppressing in Light fields," in *Proc. IEEE Int. Symp. Circuits Syst.(ISCAS)*, 2018.

[34] N. Liyanage, C. Wijenayake, C. Edussooriya, A. Madanayake, P. Agathoklis, L. T. Bruton, and E. Ambikairajah, "Multi-depth filtering and occlusion suppression in 4-D light fields: Algorithms and architectures," *Signal Process.*, vol. 167, pp. 1–13, Feb. 2020.

[35] S. U. Premaratne, C. U. S. Edussooriya, C. Wijenayake, L. T. Bruton, and P. Agathoklis, "A 4-D sparse FIR hyperfan filter for volumetric refocusing of light fields by hard thresholding," in *Proc. IEEE Int. Conf. Digital Signal Process.*, 2018, pp. 1–5.

[36] N. Liyanage, K. Abeywardena, S. S. Jayaweera, C. Wijenayake, C. U. S. Edussooriya, and S. Seneviratne, "Making sense of occluded scenes using light field pre-processing and deep-learning," in *Proc. IEEE Region 10 Conf. (accepted)*, 2020, pp. 1–6.

[37] S. S. Jayaweera and C. U. S. Edussooriya and C. Wijenayake and P. Agathoklis and L. T. Bruton, "Multi-Volumetric Refocusing of Light Fields," *IEEE Signal Processing Letters*, vol.28, pp. 31-35, 2021

[38] L. Bruton and N. Bartley, "Three-dimensional image processing using the concept of network resonance," *IEEE Transactions on Circuits and Systems*, vol. 32, no. 7, pp. 664–672, 1985.

[39] Y. Zhang and L. T. Bruton, "Applications of 3-D LCR networks in the design of 3-D recursive filters for processing image sequences," *IEEE Trans. on Circuits and Systems for Video Technology*, vol. 4, no. 4, pp. 369–382, 1994.

[40] P. Agathoklis and L. T. Bruton, "Practical-BIBO stability of n-dimensional discrete systems," *IEE Proc. G (Electron. Circuits and Syst.)*, vol. 130, no. 6, p. 236, 1983.

[41] N. Liyanage, C. Wijenayake, C. U. S. Edussooriya, and E. Ambikairajah, "Reduced-complexity depth filtering and occlusion suppression using modulated-sparse light fields," in *2019 IEEE International Symposium on Circuits and Systems (ISCAS)*, May 2019, pp. 1–5.

[42] K. Parhi, *VLSI Digital Signal Processing Systems: Design and Implementation*. Wiley India Pvt. Limited, 2007.

[43] A. Madanayake, R. Wimalagunaratne, D. G. Dansereau, and L. T. Bruton, "Design and FPGA-Implementation of 1st-Order 4D IIR Frequency-Hyperplanar Digital Filters," *IEEE 54th International Midwest Symposium on Circuits and Systems (MWSCAS)*, vol. 00, pp. 1–4, 2011.

[44] A. Madanayake, R. Wimalagunarathne, D. G. Dansereau, R. J. Cintra, and L. T. Bruton, "VLSI architecture for 4-D depth filtering," *Signal, Image and Video Processing*, vol. 9, no. 4, pp. 809–818, 2015.

[45] R. Wimalagunarathne, C. Wijenayake, A. Madanayake, D. G. Dansereau, and L. T. Bruton, "Integral form 4-D light field filters using Xilinx FPGAs and 45 nm CMOS technology," *Multidimensional Systems and Signal Processing*, vol. 26, no. 1, pp. 47–65, 2013.

[46] A. Madanayake, "Real-time FPGA Architectures for Space-time Frequency-planar MDSP," Ph.D. dissertation, University of Calgary, 2008.

[47] A. Madanayake, C. Wijenayake, D. G. Dansereau, T. K. Gunaratne, L. T. Bruton, and S. B. Williams, "Multidimensional (md) circuits and systems

for emerging applications including cognitive radio, radio astronomy, robot vision and imaging," *IEEE Circuits and Systems Magazine*, vol. 13, no. 1, pp. 10–43, 2013.

[48] R. Wimalagunarathne, A. Madanayake, D. G. Dansereau, and L. T. Bruton, "A Systolic-Array Architecture for First-Order 4-D IIR Frequency-Planar Digital Filters," *Proc. IEEE Int. Symp. Circuits Syst.(ISCAS)*, pp. 3069–3072, 2012.

[49] L. T. Bruton and N. Bartley, "The enhancement and tracking of moving objects in digital images using adaptive three-dimensional recursive filters," *IEEE Trans. Circuits Syst.*, vol. CAS-33, no. 6, pp. 604–612, June 1986.

[50] K. Kondo and N. Hamada, "Design of optimal filter for detecting linear trajectory signals utilizing object shape and velocity vector," *Electron. and Commun. in Japan, Part I*, vol. 83, no. 2, pp. 42–51, Feb. 2000.

[51] B. Kuenzle and L. T. Bruton, "3-D IIR filtering using decimated DFT-polyphase filter bank structures," *IEEE Trans. Circuits Syst. I*, vol. 53, no. 2, pp. 394–408, Feb. 2006.

[52] C. U. S. Edussooriya, L. T. Bruton, and P. Agathoklis, "A low-complexity 3D spatio-temporal FIR filter for enhancing linear trajectory signals," in *Proc. IEEE Int. Conf. Acoust., Speech, Signal Process.*, 2014, pp. 1165–1169.

[53] ——, "Velocity filtering for attenuating moving artifacts in videos using an ultra-low complexity 3-D linear-phase IIR filter," *Multidim. Syst. Signal Process.*, vol. 28, no. 2, pp. 597–616, Apr. 2017.

[54] C. U. S. Edussooriya, C. Wijenayake, L. T. Bruton, and P. Agathoklis, "Multidimensional spatio-temporal filters for depth-velocity filtering in light field videos," in *Proc. IEEE Int. Conf. Ind. Inf. Syst.*, 2017, pp. 1–6.

[55] C. U. S. Edussooriya, L. T. Bruton, and P. Agathoklis, "A 5-D IIR depth-velocity filter for enhancing objects moving on linear-trajectories in light field videos," in *Proc. IEEE Int. Symp. Circuits Syst.*, 2015, pp. 2381–2384.

[56] ——, "A novel 5-D depth-velocity filter for enhancing noisy light field videos," *Multidim. Syst. Signal Process.*, vol. 28, no. 1, pp. 353–369, Jan. 2017.

[57] N. Liyanage, S. S. Jayaweera, C. U. S. Edussooriya, C. Wijenayake, A. Madanayake, P. Agathoklis, L. Bruton, and E. Ambikairajah, "Multi depth-velocity filters for enhancing multiple moving objects in 5-d light field videos," in *2020 Moratuwa Engineering Research Conference (MERCon)*, 2020, pp. 230–235.

[58] C. Wijenayake, N. Liyanage, C. U. S. Edussooriya, H. Seatang, P. Agathoklis, and L. Bruton, "Design and implementation of 5-D IIR depth velocity filters for light field video processing," *IEEE Trans. Circuits Syst. II*, vol. 66, no. 7, pp. 1267–1271, Jul. 2019.

[59] L. Shao, R. Yan, X. Li, and Y. Liu, "From heuristic optimization to dictionary learning: A review and comprehensive comparison of image denoising algorithms," *IEEE Trans. Cybern.*, vol. 44, no. 7, pp. 1001–1013, 2014.

[60] P. Jain and V. Tyagi, "A survey of edge-preserving image denoising methods," *Inf. Syst. Front.*, vol. 18, no. 1, pp. 159–170, 2016.

[61] K. Dabov, A. Foi, V. Katkovnik, and K. Egiazarian, "Image denoising by sparse 3-D transform-domain collaborative filtering," *IEEE Trans. Image Process.*, vol. 16, no. 8, pp. 2080–2095, 2007.

[62] M. Maggioni, G. Boracchi, A. Foi, and K. Egiazarian, "Video denoising, deblocking, and enhancement through separable 4-D nonlocal spatiotemporal transforms," *IEEE Trans. Image Process*, vol. 21, no. 9, pp. 3952–3966, 2012.

[63] Z. Li, H. Baker, and R. Bajcsy, "Joint image denoising using light-field data," in *Proc. IEEE Int. Conf. Multimedia and Expo Workshops*, 2013, pp. 1–6.

[64] A. Sepas-Moghaddam, P. L. Correia, and F. Pereira, "Light field denoising: exploiting the redundancy of an epipolar sequence representation," in *Proc. IEEE 3DTV Conf.*, 2016, pp. 1–4.

[65] M. Alain and A. Smolic, "Light field denoising by sparse 5D transform domain collaborative filtering," in *Proc. IEEE Int. Workshop on Multimedia Signal Process.*, 2017, pp. 1–6.

[66] J. Chen, J. Hou, and L.-P. Chau, "Light field denoising via anisotropic parallax analysis in a CNN framework," *IEEE Signal Process. Lett.*, vol. 25, no. 9, pp. 1403–1407, Sep. 2018.

[67] Y. Liu, N. Qi, Z. Cheng, D. Liu, Q. Ling, and Z. Xiong, "Tensor-based light field denoising by integrating super-resolution," in *Proc. IEEE Int. Conf. Image Process.*, 2018, pp. 3209–3213.

[68] P. Allain, L. Guillo, and C. Guillemot, "Light field denoising using 4D anisotropic diffusion," in *Proc. IEEE Int. Conf. Acoust., Speech, Signal Process.*, 2019, pp. 1692–1696.

[69] C. Wang, N. Qi, and Q. Zhu, "Tensor-based light field denoising by exploiting non-local similarities across multiple resolutions," in *Proc. IEEE Int. Conf. Image Process.*, 2020, pp. 1078–1082.

[70] S. U. Premaratne, "Four-dimensional sparse filters for near real-time light field processing," Master's thesis, Department of Electronic and Telecommunication Engineering, University of Moratuwa, Moratuwa, Sri Lanka, 2019.

[71] S. U. Premaratne, N. Liyanage, C. U. S. Edussooriya, and C. Wijenayake, "Real-time light field denoising using a novel linear 4-D hyperfan filter," *IEEE Trans. Circuits Syst. I, Reg. Papers*, vol. 67, no. 8, pp. 2693–2706, Aug. 2020.

[72] D. G. Dansereau, B. Girod, and G. Wetzstein, "LiFF: Light Field Features in Scale and Depth," in *Proceedings of the IEEE/CVF Conference on Computer Vision and Pattern Recognition (CVPR)*, June 2019.

[73] J. T. Vorhies, A. P. Hoover, and A. Madanayake, "Adaptive Filtering of 4-D Light Field Images for Depth-based Image Enhancement," *IEEE Transactions on Circuits and Systems II: Express Briefs*, 2020.

[74] J. T. Vorhies, "Low-complexity Algorithms for Light Field Image Processing," Master's thesis, The University of Akron, 2020.

[75] C. U. S. Edussooriya, L. T. Bruton, and P. Agathoklis, "Enhancing moving objects in light field videos using 5-D IIR adaptive depth-velocity filters," in *Proc. IEEE Pacific Rim Conf. Commun., Comput., Signal Process.*, 2015, pp. 1–5.

[76] Y. Wang, J. Yang, Y. Guo, C. Xiao, and W. An, "Selective Light Field Refocusing for Camera Arrays Using Bokeh Rendering and Superresolution," *IEEE Signal Process. Lett.*, vol. 26, no. 1, pp. 204–208, 2019.

[77] C. Shin, H. G. Jeon, Y. Yoon, I. S. Kweon, and S. J. Kim, "EPINET: A Fully-Convolutional Neural Network Using Epipolar Geometry for Depth from Light Field Images," *Proc. IEEE Comput. Soc. Conf. Comput. Vis. Pattern Recognit.*, pp. 4748–4757, 2018.

[78] K. A. Skinner and M. Johnson-Roberson, "Underwater Image Dehazing with a Light Field Camera," *IEEE Comput. Soc. Conf. Comput. Vis. Pattern Recognit. Work.*, vol. 2017-July, pp. 1775–1782, 2017.